Wind and Structures, *Vol. 17, No. 2(2013) 163-184*
DOI:http://dx.doi.org/10.12989/was.2013.17.2.163

Experimental and numerical studies of aerodynamic forces on vehicles and bridges

Yan Han[1], Jiexuan Hu[1], C.S. Cai[*1,2], Zhengqing Chen[3] and Chunguang Li[1]

[1]School of Civil Engineering and Architecture, Changsha University of Science & Technology,
Changsha, Hunan, China, 410004
[2]Department of Civil and Environmental Engineering, Louisiana State University,
Baton Rouge, USA, LA 70803
[3]Wind Engineering Research Center, College of Civil Engineering, Hunan University,
Changsha, Hunan, China, 410082

(Received July 25, 2012, Revised October 3, 2012, Accepted October 8, 2012)

Abstract. An accurate identification of the aerodynamic characteristics of vehicles and the bridge is the premise for the coupled vibration analysis of a wind-vehicle-bridge system. At present, the interaction of aerodynamic forces between the road vehicles and bridge is ignored in most previous studies. In the present study, an experimental setup was developed to measure the aerodynamic characteristics of vehicles and the bridge for different cases in a wind tunnel considering the aerodynamic interference. The influence of the wind turbulence, the wind speed, the vehicle interference, and the vehicle position on the aerodynamic coefficients of vehicles, and the influence of vehicles on the static coefficients of the bridge were investigated, based on the experimental results. The variations in the aerodynamic characteristics of vehicles and the bridge were studied and the measured results were validated according to the results of surface pressure measurements on the vehicle and the bridge. The measured results were further validated by comparing the measured results with values derived numerically. The measured results showed that the wind turbulence, the vehicle interference, and the vehicle position significantly affected the aerodynamic coefficients of vehicles. However, the influence of the wind speed on the aerodynamic coefficients of the studied vehicle is small. The static coefficients of the bridge were also significantly influenced by the presence of vehicles.

Keywords: wind-vehicle-bridge system; cross winds; aerodynamic characteristics; aerodynamic interference; wind- tunnel tests; numerical simulation

1. Introduction

Economic and social developments increase tremendously the traffic volume over bridges and roads. Heavy road vehicles on bridges may significantly change the local dynamic behavior and affect the fatigue life of the bridge. On the other hand, the vibrations of bridges under cross winds also in turn affect the safety of the road vehicles. These inevitably increase the potential risk of road vehicles moving on a bridge and subjected to strong winds. Thus, it is important to study the

---

[*] Corresponding author, Professor, E-mail: cscai@lsu.edu

http://www.techno-press.org/?journal=was&subpage=8 ISSN: 1226-6116 (Print), 1598-6225 (Online)

dynamic interaction between the bridge, road vehicles, and wind loads in order to ensure the safety and normal working performance of both the road vehicles and bridge. Most existent research works focus on either wind action on vehicles running on roadway (Baker 1986, 1987, 1988, 1991a,b), wind effect on the bridge without considering vehicles (Scanlan 1990), or vehicle-bridge interaction analysis without considering the wind effect (Yang 1997, Pan 2002).

To more accurately estimate the response of a bridge and the safety of the vehicles moving on the bridge under cross winds, it is necessary to establish an analytical framework for studying the vehicle-bridge-wind interaction. Xu *et al*. (2003) have investigated the coupled dynamic analysis of road vehicles and cable-stayed bridge system under turbulent wind. Cai and Chen (2004) have built a framework for the vehicle-bridge-wind aerodynamic analysis, which lays a very important foundation for road vehicle accident analysis based on dynamic analysis results and facilitates the aerodynamic analysis of bridges considering the vehicle-bridge-wind interaction. Han and Chen (2007) also presented a state of the art three-dimensional dynamic model for the wind-vehicle-bridge coupled vibration.

However, the aerodynamic forces on vehicles in previous studies were either built on the work undertaken by Baker (1991a,b) or obtained from wind-tunnel tests, which did not consider the interaction of the aerodynamic forces between the road vehicles and the bridge.

The aerodynamic force coefficients of vehicles under wind loads depend on not only the shapes of vehicles but also those of infrastructures, such as the bridge. On the other hand, the aerodynamic parameters of the bridge will be influenced by the vehicles on it. Therefore, in order to predict the performance of the vehicle-bridge system under wind loads rationally, it is necessary to study the aerodynamic properties of road vehicles and bridges considering the interaction of the aerodynamic forces between the road vehicles and the corresponding bridges. There is a wealth of data pertaining to the wind load coefficients for vehicles on standard ‘open ground’ scenario (Baker 1991a, Quinn *et al.* 2007). However, the corresponding data for bridge decks with vehicles is sparse. Coleman and Baker (1990, 1994) measured the load coefficients of an articulated lorry positioned on the bridge deck model. Minoru Suzuki *et al*. (2003) carried out three kinds of wind tunnel tests to evaluate the aerodynamic characteristics of typical configurations of vehicles on typical configurations of infrastructures such as bridges and embankments. However, the load coefficients of the bridge deck model were not presented. Li *et al*. (2004) developed a separation device, called the Cross Slot System, to measure the aerodynamic characteristics of the rail vehicle-bridge system, taking aerodynamic interaction between the rail vehicle and the bridge into account. Cheli *et al.* (2004, 2006) undertook much work on the aerodynamic effects of rail vehicles. Though these studies (Li *et al.* 2004, 2005, 2012, Cheli *et al*. 2004, 2006) aimed at rail vehicles, the methodology can be similarly used for road vehicles. Han *et al.* (2011) calculated the load coefficients for a car container running on the bridge and the load coefficients of the bridge were also investigated by using numerical simulations (CFD).

This paper describes an experimental technique and a series of wind tunnel experiments to examine the aerodynamic characteristics of vehicles and bridge in the HD-2 wind tunnel at Hunan University, China. It is a low-speed, close-circuit medium-sized boundary layer wind tunnel, with two parallel test sections. All the measurements were undertaken in static conditions (i.e., without vehicle movement) over a range of yaw angles from 0^o~90^o. The tests were carried out in both smooth flow and high turbulence flow simulated by a turbulence producing grid.

The experimental set-up adopted for the wind tunnel tests is outlined in Section 2, which illustrates the bridge deck and vehicle geometries and the instrumentation, test conditions and testing procedure, and the characteristics of the simulated wind. Section 3 reports and examines the values of the aerodynamic force/moment coefficients of the vehicles and the bridge corresponding to a variety of test configurations. More specifically, the six studied cases are presented and compared. Section 4 describes the methodology of numerical simulations and a further comparison to the experimental results is included. Finally, some conclusions are drawn in Section 5. It is found that the wind turbulence, the vehicle interference, and the vehicle position significantly affect the aerodynamic coefficients of vehicles. However, the influence of the wind speed on the aerodynamic coefficients of the studied vehicle is small. The static coefficients of the bridge are also significantly influenced by vehicles.

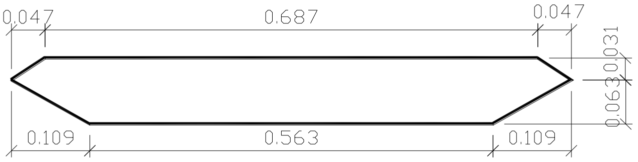

(a) Bridge cross section model

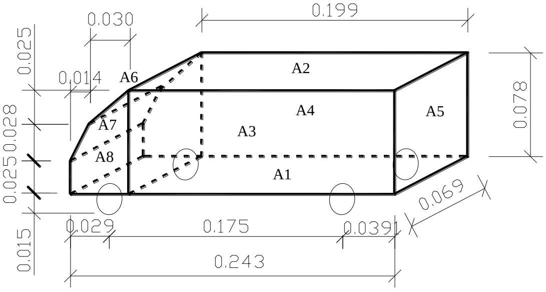

(b) Vehicle model

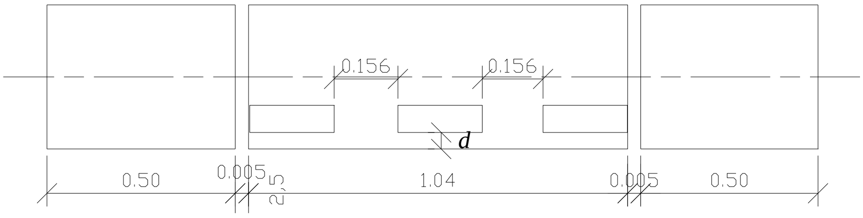

(c) Layout plan of the model

Fig. 1 Model geometry and overall dimensions (Unit: m)

2. Wind tunnel experiments

2.1 Bridge deck and vehicle geometries

The models are made with polymethylmethacrylate and the scale is 1:32. The bridge section model is divided into three parts. The intermediate part is the testing model with a length of 1.04 m. The two terminal parts are the compensation models with a length of 0.5 m, the role of which is to avoid the flow disturbance around the ends (i.e., to reduce end effects) and to improve the test precision. The gap between the intermediate part and the terminal part is 0.005 m. The details and dimensions of the bridge deck section and the vehicle are given in Figs. 1(a) and 1(b). The distance between the bottom of the vehicle and the top surface of the bridge deck is 0.015 m. The distance of the vehicle from the bridge deck windward edge is defined by *d* with the values of 0.166 m or 0.547 m corresponding to the two different transverse positions of the vehicle on the bridge deck, windward and leeward lanes, as shown in Fig. 1(c). Three vehicles are made to investigate the aerodynamic interference between vehicles, which are laid on the bridge deck with an equal distance of 0.156 m between vehicles along the longitudinal direction, as shown in Fig. 1(c). The middle vehicle model is the test vehicle and the terminal vehicle models are used to simulate the interference of vehicles.

Fig. 2 Experimental setup

2.2 Experimental set-up

The experimental set-up is composed of three test frames, the middle test frame and the two end compensation frames, as shown in Fig. 2, each of which is composed of three parts, the upper, the middle, and the lower parts. The upper part fixes the model to the test frame by using bolts. The middle part is the circular steel tube with a little smaller diameter, the top of which is connected with the upper part by using bolts and the end is inserted into the circular steel tube of the lower part and fixed with the lantern ring. The lower part is a composite structure consisting of a circular steel tube with a larger diameter and a steel bar. The lower part is connected with the rotating table in the wind tunnel by using bolts. In the experimental process, the test frames and the models are rotated with the table together to vary the wind yaw angle.

2.3 Turbulence wind field simulation

A passive turbulence generator was developed for generating turbulence wind field, as shown in Fig. 3. The characteristics of the generated flow in the wind tunnel were measured by a TFI Series 100 cobra probes (Turbulent Flow Instrumentation). The wind turbulence intensity at the deck height was approximately 10% in the flow direction. The longitudinal integral scale for the streamwise wind velocity was 0.5 m which is well above the vehicle height (or length or width); thus ensuring that the turbulence structures are well correlated over the vehicles.

Fig. 4 indicates the power spectral density of the approaching streamwise wind velocity. To facilitate a comparison between the wind tunnel simulation and the target spectrum at a full scale (i.e., the Von Karman Spectrum) both the horizontal and vertical axes in Fig. 4 have been non-dimensionalized. The horizontal axis represents the reduced frequency ($\overline{f} = f.L_u / U$) defined by the product of the frequency (*f*) and the turbulence length scale (L_u), divided by the reference mean wind speed. On the vertical axis the spectrum is multiplied by the frequency and divided by the mean velocity variance. The experimental and target spectra agree qualitatively well over a large proportion of the reduced frequency range, which suggests that the turbulence simulation is sufficient for the current purposes.

Fig. 3 Passive grid device

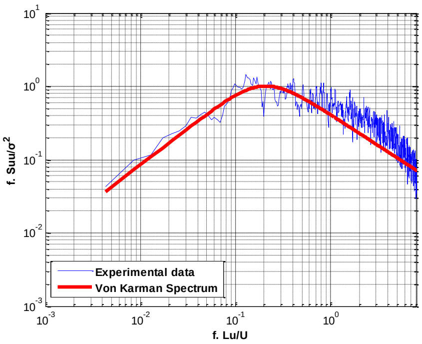

Fig. 4 Power spectral density of the longitudinal wind turbulence

2.4 Force measurements

The forces on the bridge and the vehicle were determined by integrating the measured tap pressure. The bridge model was installed with 329 pressure taps, mounted flush with the surfaces of the bridge model and connected to the pressure transducers via flexible tubing. Seven pressure-tapped strips were located along the span of the bridge deck, as shown in Fig. 5(a), to take into account the span-wise correlation of the aerodynamic forces. Each pressure-tapped strip has 47 pressure taps representing the surface pressure distributions, as shown in Fig. 5(b). The vehicle model was installed with 200 pressure taps, as shown in Fig. 6. Figs. 7 and 8 outline the sign conventions for the aerodynamic forces of the bridge and the vehicle, respectively.

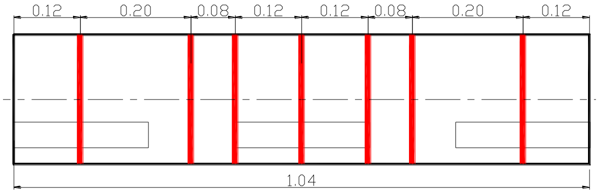

(a) Positions of seven pressure-tapped strips (Unit: m)

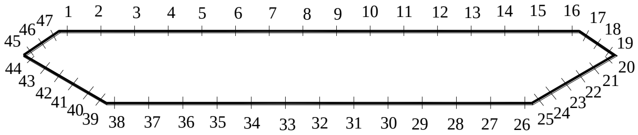

(b) Positions of pressure taps for each pressure-tapped strip

Fig. 5 Sketch map of pressure taps of the bridge cross section

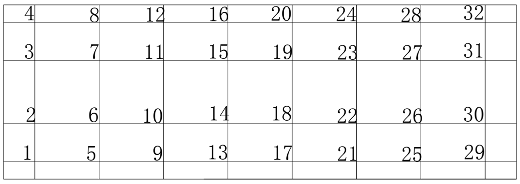

(a) Top surface

(b) Frontal surface (c) Back surface

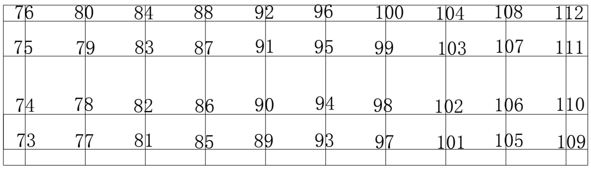

(d) Bottom surface

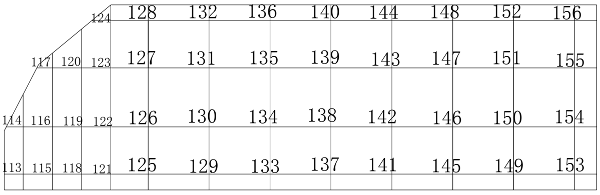

(e) Left side surface

Continued

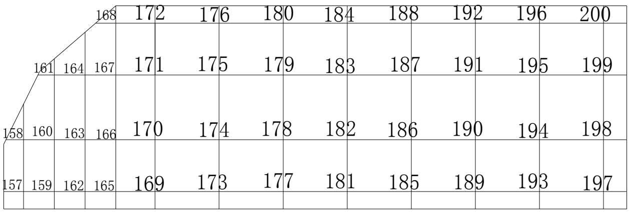

(f) Right side surface

Fig. 6 Positions of pressure taps for each surface of the vehicle

The instantaneous fluctuating surface pressure at time t in a particular strip (j=1-7) were integrated independently over each of the seven pressure-tapped strips. The lift force $F_{Vj}(t)$, drag force $F_{Hj}(t)$, and pitching moment $M_j(t)$ per unit span length of the bridge deck were calculated according to Eqs. (1(a)), (1(b)) and (1(c)), respectively, as

$$F_{Vj}(t) = \sum_{i=1}^{47} p_{ij}(t)\Delta A_{ij} \cos(\alpha_{ij}) \tag{1a}$$

$$F_{Hj}(t) = \sum_{i=1}^{47} p_{ij}(t)\Delta A_{ij} \sin(\alpha_{ij}) \tag{1b}$$

$$M_j(t) = \sum_{i=1}^{47} p_{ij}(t)\Delta A_{ij} d_{Hij} \sin(\alpha_{ij}) + \sum_{i=1}^{47} p_{ij}(t)\Delta A_{ij} d_{Vij} \cos(\alpha_{ij}) \tag{1c}$$

where p_{ij} (t) = the instantaneous fluctuating surface pressure of the bridge at time t; ΔA_{ij} = the tributary area of a pressure tap of the bridge; α_{ij} = angle between the local (pressure tap) and vertical axis; and d_{Hij} , d_{Vij} = pitching moment arms about the center of the bridge deck.

Similarly, the instantaneous fluctuating surface pressures at time t were integrated independently over each surface of the vehicle. The side force $F_S(t)$, lift force $F_L(t)$, drag force $F_D(t)$, pitching moment $F_P(t)$, yawing moment $F_R(t)$, and rolling moment $F_R(t)$ of the vehicle were calculated according to Eqs. (2(a)), (2(b)) and (2(c)), respectively, as

$$F_S(t) = \sum_{i=1}^{200} p_i(t)\Delta A_i \Theta_{Si} \tag{2a}$$

$$F_L(t) = \sum_{i=1}^{200} p_i(t)\Delta A_i \Theta_{Li} \tag{2b}$$

$$F_D(t) = \sum_{i=1}^{200} p_i(t)\Delta A_i \Theta_{Di} \tag{2c}$$

$$F_P(t) = \sum_{i=1}^{200} p_i(t)\Delta A_i \Theta_{Li} d_{(L\text{-}S)i} + \sum_{i=1}^{200} p_i(t)\Delta A_i \Theta_{Di} d_{(D\text{-}S)i} \tag{2d}$$

$$F_Y(t)=\sum_{i=1}^{200}p_i(t)\Delta A_i\Theta_{Si}d_{(S\text{-}L)i}+\sum_{i=1}^{200}p_i(t)\Delta A_i\Theta_{Di}d_{(D\text{-}L)i} \tag{2e}$$

$$F_R(t)=\sum_{i=1}^{200}p_i(t)\Delta A_i\Theta_{Li}d_{(L\text{-}D)i}+\sum_{i=1}^{200}p_i(t)\Delta A_i\Theta_{Si}d_{(S\text{-}D)i} \tag{2f}$$

where $p_i(t)$ = the instantaneous fluctuating surface pressure of the vehicle at time t; ΔA_i = the tributary area of a pressure tap of the vehicle; Θ_{Fi} ($_F$ = S, L, D) = the decomposition coefficients of surface pressure along the direction of side, lift, or drag force; $d_{(L\text{-}S)i}$ and $d_{(D\text{-}S)i}$ = horizontal moment arms of the lift force and vertical moment arm of the drag force contributing to the pitching moment, respectively; $d_{(S\text{-}L)i}$ and $d_{(D\text{-}L)i}$ = horizontal moment arms of the side force and horizontal moment arm of the drag force contributing to the yawing moment, respectively; and $d_{(S\text{-}D)i}$ and $d_{(L\text{-}D)i}$.= vertical moment arm of the side force and horizontal moment arms of the lift force contributing to the rolling moment, respectively.

Based on the integrated lift force, drag force, and pitching moment, the corresponding force and moment coefficients of the bridge were determined according to Eqs. (3(a)), (3(b)) and (3(c)), respectively, as

$$C_{F_H}=\frac{1}{7}\sum_{j=1}^{7}\frac{\overline{F}_{Hj}}{0.5\rho U^2B} \tag{3a}$$

$$C_{F_V}=\frac{1}{7}\sum_{j=1}^{7}\frac{\overline{F}_{Vj}}{0.5\rho U^2B} \tag{3b}$$

$$C_{M}=\frac{1}{7}\sum_{j=1}^{7}\frac{\overline{M}_{j}}{0.5\rho U^2B^2} \tag{3c}$$

where ρ = the air density; U = the mean wind speed on the elevation of the bridge; $\overline{F}_{Hj}$, $\overline{F}_{Vj}$ and $\overline{M}_j$ = the time averaged values of the lift force, drag force, and pitching moment in Eqs. (1(a)), (1(b)) and (1(c)) over the required time period for strip j; and B = the width of the bridge deck.

Based on the integrated side force, lift force, drag force, pitching moment, yawing moment, and rolling moment, the corresponding force and moment coefficients of the vehicle were determined according to Eqs. (4(a))-(4(f)), respectively, as

$$C_S(\psi)=\frac{\overline{F}_S}{0.5\rho V^2A} \tag{4a}$$

$$C_L(\psi)=\frac{\overline{F}_L}{0.5\rho V^2A} \tag{4b}$$

$$C_D(\psi)=\frac{\overline{F}_D}{0.5\rho V^2A} \tag{4c}$$

$$C_P(\psi) = \frac{\overline{F}_P}{0.5\rho V^2 Ah} \tag{4d}$$

$$C_Y(\psi) = \frac{\overline{F}_Y}{0.5\rho V^2 Ah} \tag{4e}$$

$$C_R(\psi) = \frac{\overline{F}_R}{0.5\rho V^2 Ah} \tag{4f}$$

where $\overline{F}_S, \overline{F}_L, \overline{F}_D, \overline{F}_P, \overline{F}_Y$ and $\overline{F}_R$ = the time averaged values of the side force, lift force, drag force, pitching moment, yawing moment, and rolling moment in Eqs. (2(a))-(2(f)) over the required time period; A= frontal area of the vehicle; h is the distance from the gravity center of the vehicle to the road surface; and V is the relative wind speed to the vehicle, of which the specification is shown in Fig. 9.

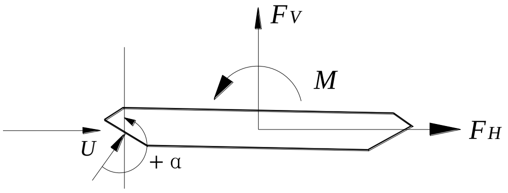

Fig. 7 Sign convention for aerodynamic forces of the bridge

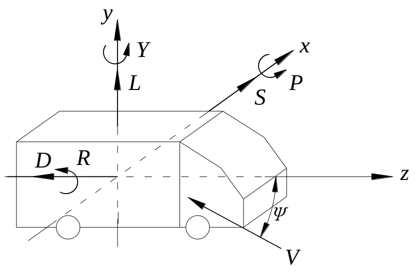

Fig. 8 Sign convention for aerodynamic forces of the vehicle

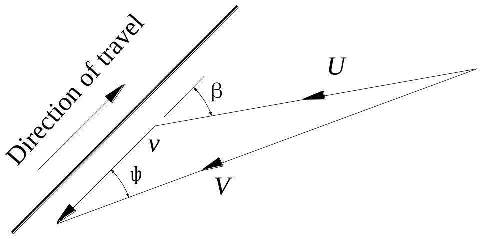

Fig. 9 Velocities and directions

In Fig. 9, v is the vehicle speed; ψ is the relative wind yaw angle to the vehicle; β is the angle between the wind direction and the vehicle direction of travel, and $\psi=\beta$ in this paper since no vehicle movement is considered.

2.5 Test configurations and experimental procedure

Table 1 outlines the experimental configurations examined in the current work. In order to vary the yaw angle for the vehicle, the bridge and vehicle were simply rotated with respect to the oncoming wind together with the test frame and the rotating table in the wind tunnel. Seven yaw angles of 0^o, 15^o, 30^o, 45^o, 60^o, 75^o and 90^o were investigated. To investigate the influence of wind velocity, two velocities of 10 m/s and 20 m/s were adopted. Three vehicles were laid on the bridge deck with an equal distance of 0.156 m between the vehicles along the longitudinal direction to investigate the aerodynamic interference between the vehicles. The tests were carried out in smooth flow and turbulent flow with approximately a 10% turbulence intensity as described in Section 2.3. The local wind field of the surface of the bridge deck is expected to be modified due to the existence of the vehicles. Also, the local wind field of the vehicle is expected to be modified as a result of the existence of the bridge. The vehicle model was positioned at two different locations corresponding to windward and leeward lanes.

Table 1 Measured cases in wind tunnel

Cases	Testing objects	Wind Velocity (m/s)	Wind field	Distance (d) of vehicle from the windward edge of the deck (m)	Wind yaw angle (^{o})
1	Bridge with one vehicle	10	Smooth	0.166	0, 15, 30, 45, 60, 75, 90
2	Bridge with one vehicle	20	Smooth	0.166	0, 15, 30, 45, 60, 75, 90
3	Bridge with one vehicle	10	Smooth	0.547	0, 15, 30, 45, 60, 75, 90
4	Bridge with one vehicle	10	Turbulent	0.166	0, 15, 30, 45, 60, 75, 90
5	Bridge with three vehicles	10	Smooth	0.166	0, 15, 30, 45, 60, 75, 90
6	Bridge with no vehicle	10	Smooth	0	0, 15, 30, 45, 60, 75, 90

3. Experimental results and discussion

3.1 Aerodynamic force coefficients

Fig. 10 illustrates the variation of force and moment coefficients of the vehicle with respect to the yaw angle ψ for Cases 1(one vehicle) and 5 (three vehicles). It can be seen that for Case 1, the side force coefficient C_S increases with the increase of the yaw angle ψ and reaches a maximum value at around 90^o yaw angle. However, the increment between the yaw angles of 60-90 degrees is less significant. Such a trend is similar to that reported in the literature (Baker 1991a, Coleman

1990), although it is noted that the maximum values typically occur between yaw angles of 60-90 degrees. The lift force coefficient C_L increases and then decreases with the increase of the yaw angle ψ, and reaches a maximum value at around 30^o yaw angle. Its value is positive for $15^o<\psi<60^o$, and negative for the other yaw angles. The positive values (sign convention shown in Fig. 8) of C_L are not good for traffic safety. The magnitude of the drag force coefficient C_D increases to a maximum at $\psi=30^o$ and then decreases to near zero for $\psi=90^o$, i.e., a pure cross wind condition, which seems reasonable. The aerodynamic moments reflect the trends of the aerodynamic forces. As for the pitching moment coefficient C_P, though the data is scattered for $\psi<60^o$, there is a distinct change trend for $60^o<\psi<90^o$, i.e., decreasing with the increase of the yaw angle ψ. The yawing moment coefficient C_Y shows similar variations to those observed in C_P. The rolling moment coefficient C_R decreases with the increase of the yaw angle ψ obviously and the values are negative.

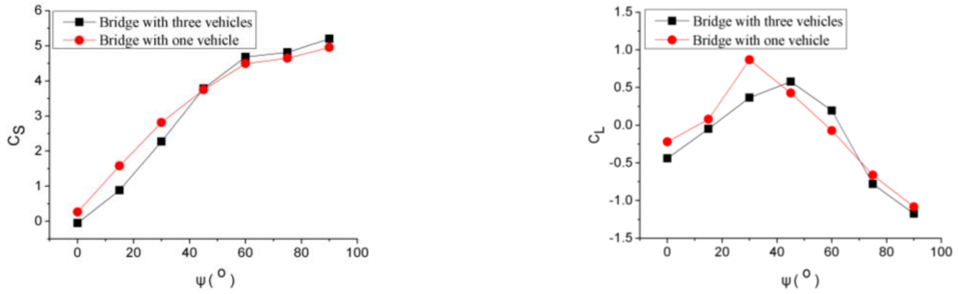

(a) Side force coefficient (b) Lift force coefficient

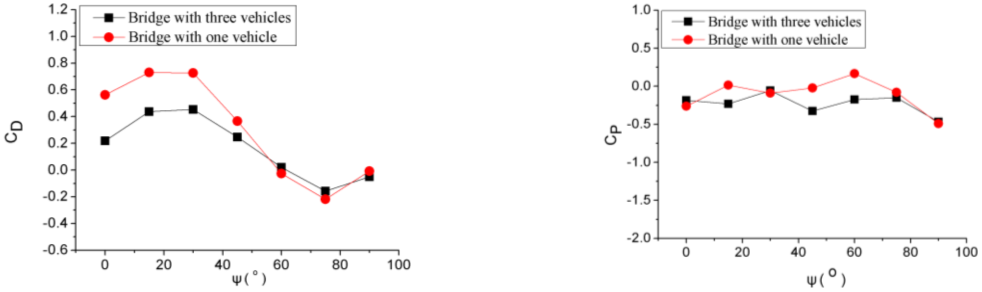

(c) Drag force coefficient (d) Pitching moment coefficient

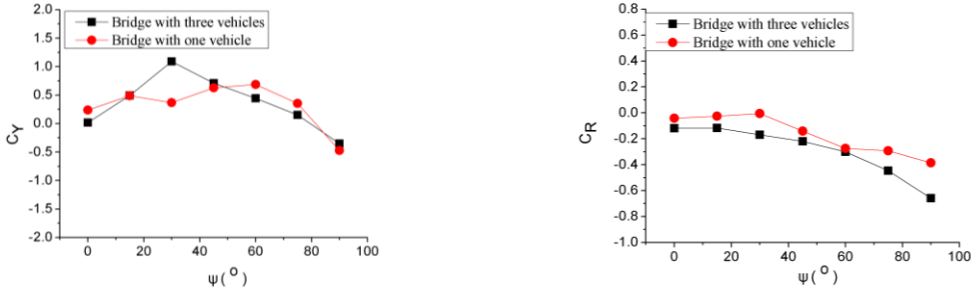

(e) Yawing moment coefficient (f) Rolling moment coefficient

Fig. 10 Aerodynamic force coefficients of the vehicle vs. yaw angle ψ for Cases 1 and 5

In addition, from the comparison of the results for Cases 1 and 5 (one vs. three vehicles in Fig. 10), it can be seen that the change trend of the aerodynamic coefficients is similar for the two cases. The side force coefficient C_S in Case 5 with three vehicles is obviously less than that in Case 1 with one vehicle for $\psi<45^{\circ}$ because of the blocking effect of the frontal vehicle on the middle vehicle, i.e., the test vehicle. When the blocking effect is not obvious for $\psi>45^{\circ}$, the side force coefficient C_S for Case 5 is slightly larger than that in Case 1 due to the effect of the frontal and posterior vehicles on the surrounding flow field. There is an obvious difference in the lift force coefficient C_L between Cases 1 and 5, especially for 30° yaw angle, at which the lift force coefficient C_L for Case 5 is obviously less than that in Case 1, which means the effect of frontal and posterior vehicles is good for traffic safety of the middle vehicle. The frontal vehicle affects the drag force coefficient C_D greatly, which reduces the magnitude of the drag force coefficient C_D, especially for $\psi<60^{\circ}$. The interference of frontal and posterior vehicles affects the pitching moment coefficient C_P greatly for $\psi=15^{\circ}$, 45° and 60°, but there is no effect for other yaw angles. The interference affects the yawing moment coefficient C_Y relatively small, except for 30° yaw angle. The absolute value of the rolling moment coefficient C_R in Case 5 with three vehicles is larger than that in Case 1 with one vehicle for all yaw angles due to the interference of the frontal and posterior vehicles.

(a) Side force coefficient (b) Lift force coefficient

(c) Drag force coefficient (d) Pitching moment coefficient

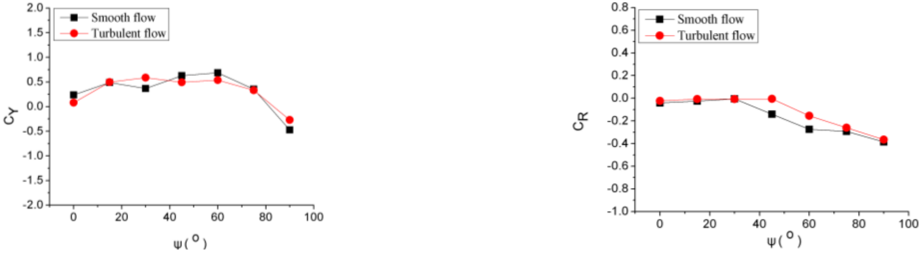

(e) Yawing moment coefficient (f) Rolling moment coefficient

Fig. 11 Aerodynamic force coefficients of the vehicle vs. yaw angle ψ for Cases 1 and 4

Fig. 11 illustrates the variation of the aerodynamic force coefficients of the vehicle with respect to yaw angle ψ for Cases 1and 4 (smooth vs. turbulent flow). It can be seen that the side force coefficient C_S for turbulent flow is smaller than that in the smooth flow and the difference increases with the increase of the yaw angle. The turbulence effect on the lift force coefficient C_L is not obvious for low yaw angles. For $\psi>40^o$, the lift force coefficient C_L in turbulent flow is significantly greater than that in the smooth flow case. The magnitude of the drag force coefficient C_D for the turbulent flow is smaller than that in the smooth flow for $\psi<45^o$, and slightly greater for $\psi>45^o$. The effect of the turbulence on the moment coefficients is small relative to the force coefficients. The pitching moment coefficient C_P in turbulent flow is less than that in the smooth flow for all yaw angles, especially for 45^o yaw angle. The rolling moment coefficient C_R in turbulent flow is larger than that in the smooth flow for $\psi=45^o$ and 60^o, but there is no change for other yaw angles. The turbulence affects the yawing moment coefficient C_Y relatively small and irregularly.

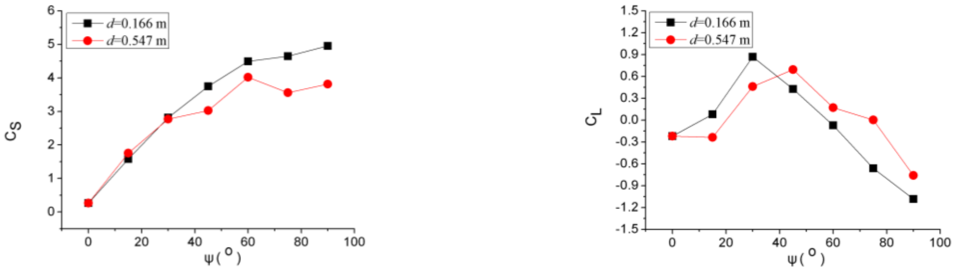

(a) Side force coefficient (b) Lift force coefficient

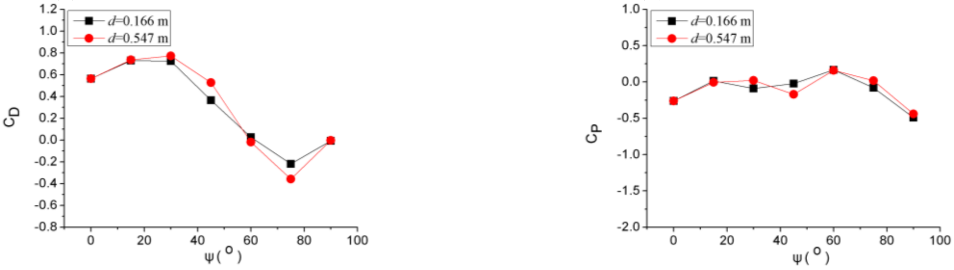

(c) Drag force coefficient (d) Pitching moment coefficient

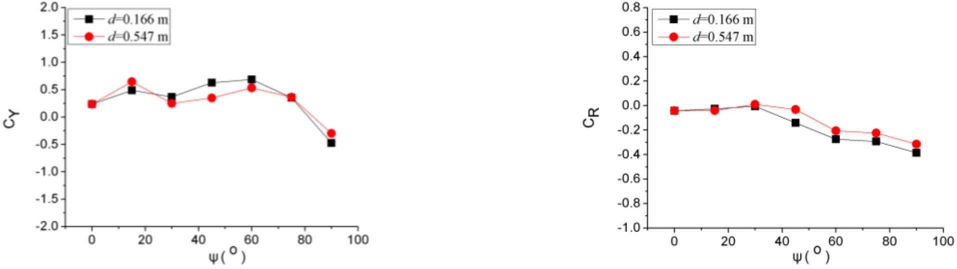

(e) Yawing moment coefficient (f) Rolling moment coefficient

Fig. 12 Aerodynamic force coefficients of the vehicle vs. yaw angle ψ for Cases 1 and 3

A further investigation on the influence of the vehicle position on the aerodynamic force coefficients is illustrated in Fig.12 which shows the evolution of the aerodynamic coefficients with respect to the two distances (i.e., d=0.166 m and 0.547 m corresponding to Cases 1 and 3). For all coefficients, there is no difference between the results for d=0.166 m and 0.547 m at 0^{o} yaw angle, which is reasonable because the flow disturbance on the vehicle is same whether for d=0.166 m or d=0.547 m when $\psi=0^{o}$. For $\psi<30^{o}$, there is a good agreement between the results of the side force coefficient C_S in the two cases. However, the increase of the distance d reduces C_S greatly for $\psi>30^{o}$. The lift force coefficient C_L decreases with the increase of the distance d for $\psi<40^{o}$ except for $\psi=0^{o}$, and increases with the increase of the distance d for $\psi>40^{o}$. The changing of the distance affects the drag force, pitching moment, yawing moment, and rolling moment coefficients insignificantly.

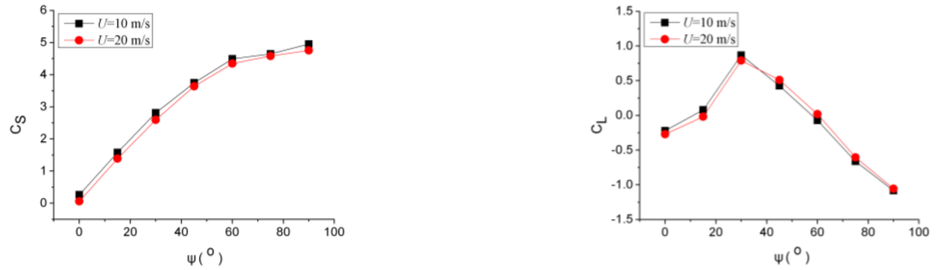

(a) Side force coefficient (b) Lift force coefficient

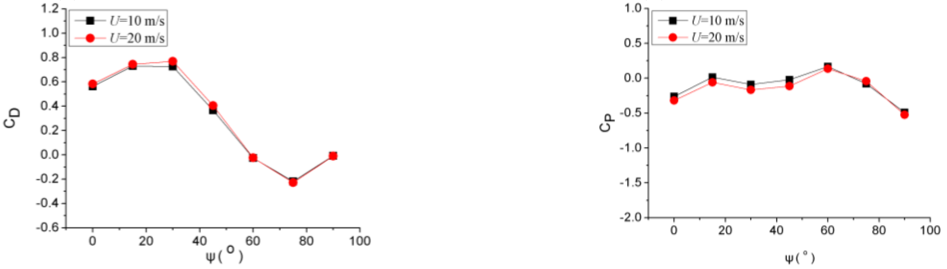

(c) Drag force coefficient (d) Pitching moment coefficient

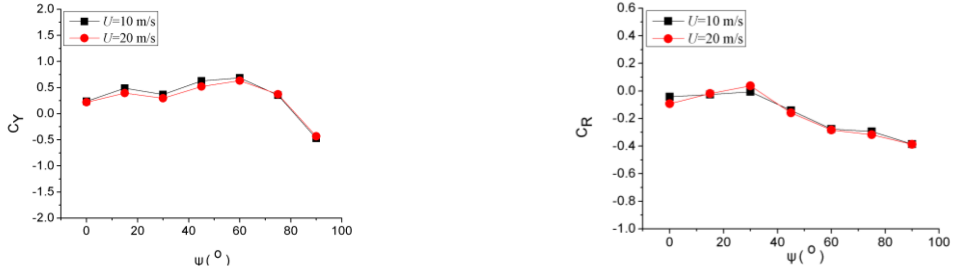

(e) Yawing moment coefficient (f) Rolling moment coefficient

Fig. 13 Aerodynamic force coefficients of the vehicle vs. yaw angle ψ for Cases 1 and 5

Fig. 13 shows the variation of the aerodynamic force coefficients of the vehicle with respect to the yaw angle ψ for Cases 1 and 2 (10 vs. 20 m/s wind velocity) to investigate the effect of the wind speed on the coefficients. It can be seen that there is very little difference between the results for all the aerodynamic force coefficients, which is perhaps not surprising since the vehicle model has sharp windward edges. As a result, the coefficients will not be sensitive to the Reynolds number (i.e., the wind velocity here).

Table 2 gives the static aerodynamic force coefficients of the bridge for Cases 6, 1, 5 and 3 at the 90^o yaw angle. The results show that the aerodynamic force coefficients of the bridge are affected by the vehicles greatly, especially for the lift force coefficient C_V, which increases significantly with the increase of the vehicle number. The drag force coefficient C_H with one vehicle is obviously greater than that with no vehicle, but slightly smaller than that with three vehicles. The magnitude of the pitching moment coefficient C_M with three vehicles is significantly greater than that with one vehicle or with no vehicle, but there is small difference between the results with one vehicle and with no vehicle. The distance of the vehicle from the windward edge of the bridge deck d affects the aerodynamic force coefficients of the bridge greatly. It not only affects the magnitude but also the direction of the lift force coefficients. The magnitudes of the drag force and pitching moment coefficients for d = 0.547 m are obviously larger than those for d = 0.166 m.

Table 2 Static coefficients of the bridge

Coefficients	With no vehicle	With one vehicle (d=0.166 m)	With three vehicles (d=0.166 m)	With one vehicle (d=0.547 m)
C_V	0.1486	0.2602	0.3287	-0.0983
C_H	0.0583	0.0669	0.0672	0.0830
C_M	-0.0175	-0.0141	-0.0341	-0.0445

3.2 Pressure distribution

A further investigation on the cause of changes of the aerodynamic forces for the vehicle and the bridge is illustrated in Figs. 14-16, showing the surface pressure distribution of the vehicle and the bridge. Fig. 14 gives the pressure contour of the windward side surface of the vehicle at the 90^o yaw angle for Cases 1, 4, 5 and 3. Fig. 15 gives the pressure contour of the frontal surface of the vehicle at the 0^o yaw angle for Cases 1 and 5. Figure 16 shows the pressure distribution of the top pressure taps of the middle strip of the bridge deck at the 90^o yaw angle for Cases 1, 3, 5 and 6. It can be seen from these figures that all pressure taps are functioning normally since there are no abnormal values for all pressure taps.

From Figs. 14(a) and 14(c), it can be seen that there is a good agreement between the side surface pressure contour of Cases 1 and 5, which verifies that the effect of the frontal and posterior vehicles on the side force coefficient C_S is not obvious, just as shown in Fig. 10(a). By comparing Fig. 14(a) with Fig. 14(b), it can be seen that the side surface pressure for Case 4 is obviously smaller than that in Case 1, which explains the decrease of the side force coefficient C_S in turbulence flow at the 90^o yaw angle, as shown in Fig. 11(a). Though the side surface pressure in Case 3 is not smaller than that in Case 1, as illustrated in Figs. 14(a) and 14(d), the high pressure area in Case 3 becomes small, which decreases the side force coefficient C_S at the 90^o yaw angle obviously, as shown in Fig. 12(a).

As illustrated in Figs. 15(a) and 15(b), the frontal surface pressure in Case 5 is obviously smaller than that in Case 1 due to the blocking effect of the frontal vehicle, which is the main reason for the obvious decrease of the drag force coefficient C_D at the 0^o yaw angle, as shown in Fig. 10(c).

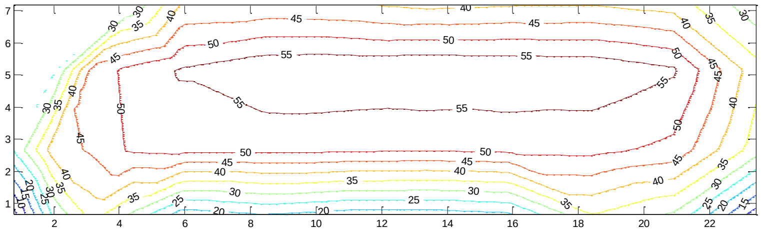

(a) Case 1

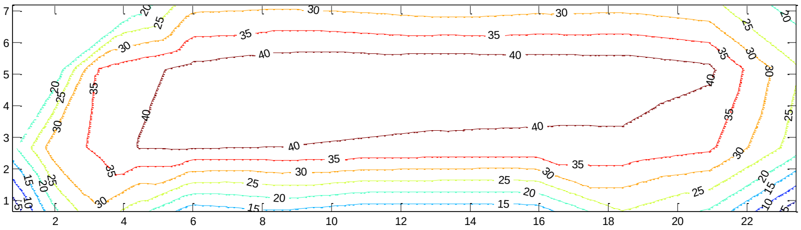

(b) Case 4

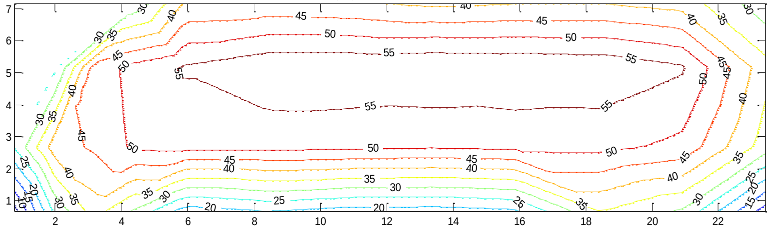

(c) Case 5

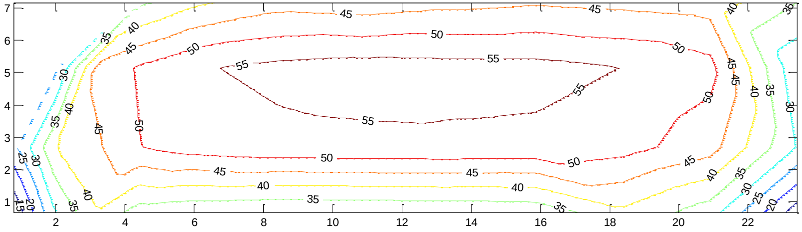

(d) Case 3

Fig. 14 Pressure contour of the windward side surface of the vehicle at 90^o yaw angle

From Fig. 16, it is observed that for Case 6 (with no vehicle), the pressure is negative, that is, the measured point is subjected to a tensile force with an upward direction (i.e., the positive direction of life force). The pressure increases (the absolute value decreases) with the increase of the distance from the windward edge and then basically remains unchanged after the distance is up to a certain value. For Case 1 (one vehicle with d=0.166 m), the pressure of the measured point located in front of the vehicle on the windward side lane increases sharply with the increase of the distance from the windward edge due to the blockage effect of the vehicle, changing from negative to positive. The pressure becomes negative when the measured point is located under the vehicle and approaches to the value like that in Case 6. The magnitude of the pressure for Case 1 is larger than that in Case 6 with the direction upward, which leads to the lift force coefficient C_V to change correspondingly. For Case 5 (with three vehicles), the variation of the pressure is similar to that in Case 1, except for the pressure taps in front of the windward side vehicle. Since there are three strips of the bridge deck (as shown in Fig. 5(a)) affected by the vehicles, the lift force coefficient C_V in Case 5 is obviously higher than that in Case 1. For Case 3 (one vehicle with d=0.547 m), the pressure increases with the increase of the distance from the windward edge, turns from negative to positive, but decreases sharply near the vehicle and becomes negative again. There are many measured points (such as points of 6, 7, 8, 9, 10, 11, 12) that have positive pressure values with a downward direction. As a result, the lift force coefficient C_V in Case 3 is negative and is lower than that in Case 6. From the above analysis, it is not hard to understand the change reason of the lift force coefficients presented in Table 2.

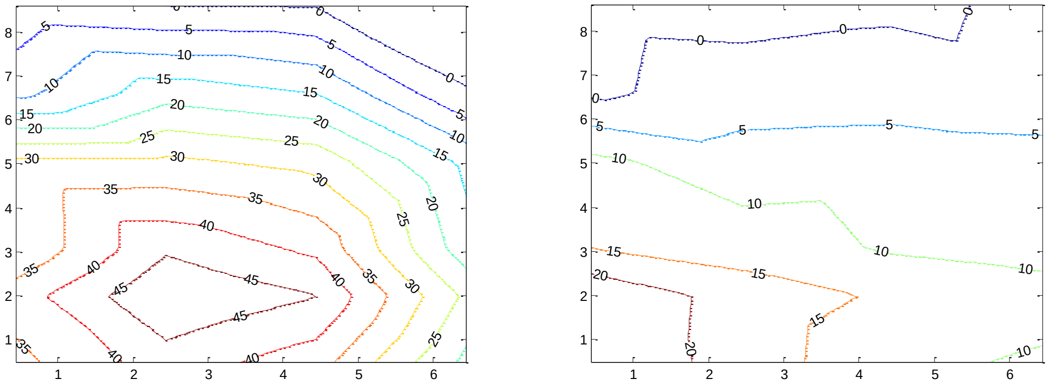

(a) Case 1 (b) Case 5

Fig. 15 Pressure contour of the frontal surface of the vehicle at 0° yaw angle

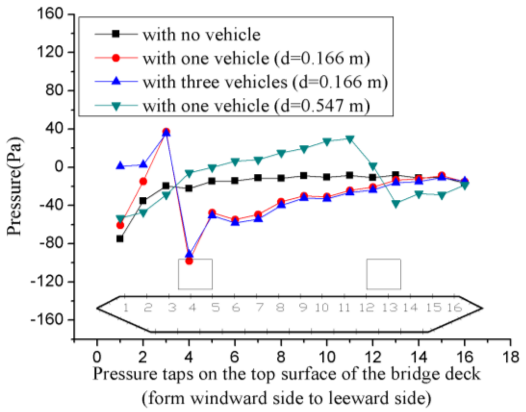

Fig. 16 Measured pressure of top pressure taps of the middle strip

4. Numerical simulation

As a cross check against the experimental measurements, Case 1 was numerically simulated using CFD method and the results were compared with the experimental ones. In this simulation, the analysis was performed using a commercial CFD solver ANSYS CFX 12. ANSYS CFX uses the Navier-Stokes equations to describe the fundamental processes of momentum, heat, and mass transfer. Like most commercial CFD packages, ANSYS CFX uses a finite volume approach to convert the governing partial differential equations into a system of discrete algebraic equations by discretizing the computational domain. These equations may result in a solution with specified domain boundary conditions.

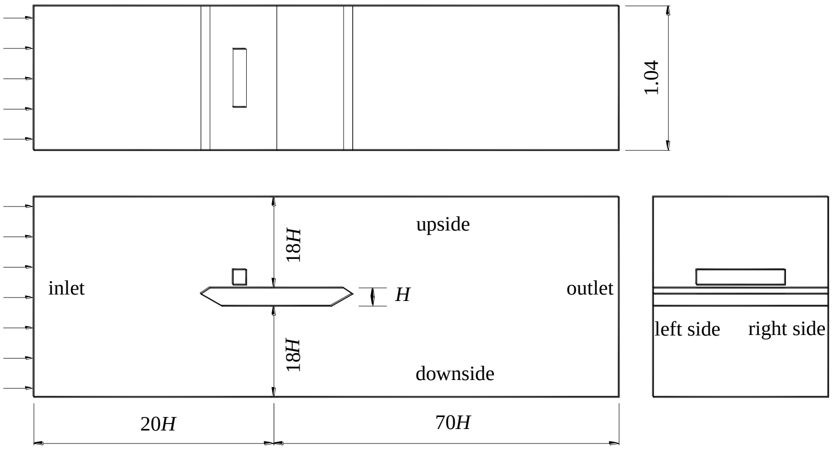

Fig. 17 Computational domain used in the simulations

4.1 Simulation method

The present flow is inherently unsteady, not only because of the flow turbulence, but also because of the large scale vortex shedding present in the separated wake behind the vehicle and the bridge. The Reynolds averaged Navier Stokes (RANS) method is used to simulate the flow around the vehicle and bridge and it is capable of modeling this flow comprehensively.

The choice of a turbulence model as part of the RANS modeling is important and can influence the results quite considerably. The Shear Stress Transport (SST) turbulence model is applied to represent the turbulence of the flow. The model is designed to deal with adverse pressure gradients and separated flows and thus performs well for the present flow problem. Part of the reason that the SST model does well is the way the model deals with the boundary layer. The SST model differs from other RANS models because of its resolution of the flow in the boundary layer. The boundary layer is resolved by using very small mesh length scales in the direction normal to the wall. Although this allows for a detailed analysis of the boundary layer, it increases the computation expense of the model due to the mesh inflation layers used close to the wall. However, the SST model remains a two-equation model and the cost still remains acceptable.

In this study, the meshes were built using ICEM provided by ANSYS. y^+ values on the vehicle and bridge surfaces were within that of the SST turbulence model specification. A typical value of y^+=1 was aimed at and achieved for most of the vehicle and bridge surfaces.

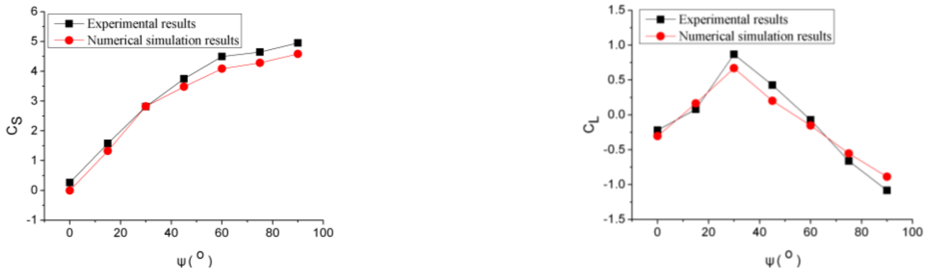

(a) Side force coefficient (b) Lift force coefficient

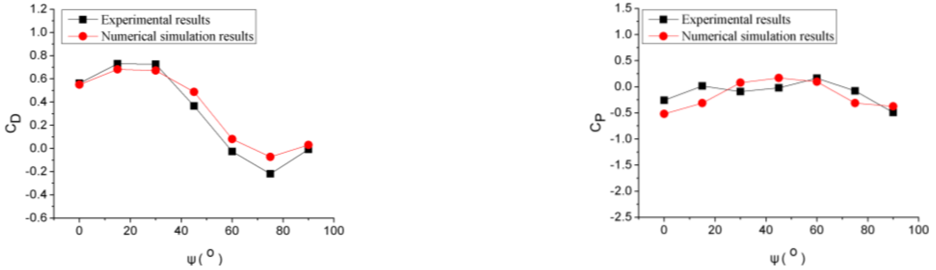

(c) Drag force coefficient (d) Pitching moment coefficient

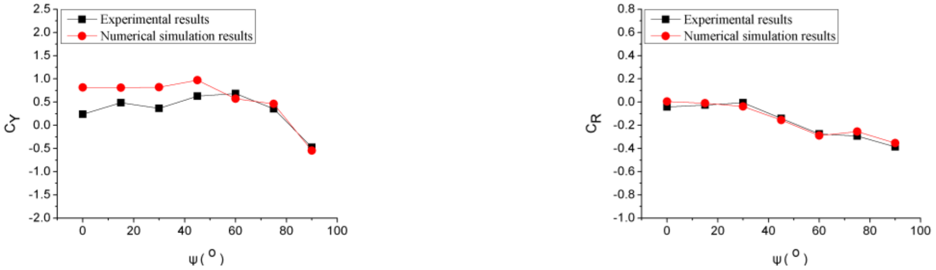

(e) Yawing moment coefficient (f) Rolling moment coefficient

Fig. 18 Experimental and numerical results of the vehicle for Case 1

4.2 Computational domain and boundary conditions

The three-dimensional computational model of the vehicle on the section of the bridge can be seen in Fig. 17. The depth of the bridge *H* is chosen as the characteristic length. The inflow boundary is located 20 *H* upstream of the center line of the bridge and the outflow boundary is 70 *H* downstream. The computational domain extends 18 *H* from the surface of the bridge on both sides. The simulated length of the bridge is 1.04 m, the same as the tested one.

In a simulation with ANSYS CFX, the atmospheric boundary is always set as an open boundary, where fluids can simultaneously flow in and out of the domain. The upside and downside are set as free-slip wall boundary conditions. The symmetry boundary conditions are employed on the left and right sides. The no-slip wall boundary conditions are applied on the surfaces of the vehicles and the bridge. The wind velocity vector, turbulence intensity and longitudinal scale can be specified at the inlet surface. The domain boundary at the inlet surface is set to be uniform wind profiles with the correct magnitude and direction.

4.3 Numerical results and comparison with experimental results

Fig. 18 shows the experimental and numerical results of the aerodynamic force coefficients of the vehicle for Case 1. It can be seen from Fig. 18, though there is a certain difference between the experimental and numerical results, the variation trend of the values is similar. Fig. 19 shows the pressure contour of the planar top plane of the bridge in Case 1. It shows that the pressure in front of the vehicle on the windward side increases from a negative value to the maximum positive pressure due to the blockage effect of the vehicle. The maximum negative pressure occurs under the vehicle, and gradually changes to a constant pressure. The changing trend of the pressure has a good agreement with that of the experimental results for Case 1 (one vehicle with d=0.166 m), as shown in Fig. 16. This good agreement cross examines the numerical and experimental results and verifies that the developed procedure can be used in more simulations for future studies.

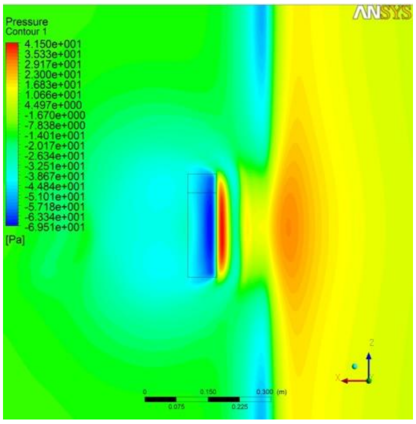

Fig. 19 Pressure contour of the planar top plane of the bridge

5. Conclusions

The present work has investigated the aerodynamic force coefficients of the vehicle and the bridge by carrying out wind tunnel tests and numerical simulating. Based on the results, the following conclusions can be drawn:

(1) The analysis of surface pressure distributions of the vehicle and bridge proves that experimental results in this paper are accurate and reliable. The experimental results agree well with the numerical results. This cross checking proves that both the experimental and numerical approaches in this paper are reliable.

(2) The aerodynamic coefficients are obviously functions of the yaw angle. The side force coefficient C_S increases with the increase of the yaw angle ψ, the lift force coefficient C_L increases and then decreases with the increase of the yaw angle ψ, the drag force coefficient C_D increases slightly and then decreases with the increase of the yaw angle ψ, the yawing moment coefficient

shows similar variations to those observed in the drag force coefficient, and the pitching moment and rolling moment results are relatively small.

(3) The interference of vehicles, the flow turbulence, and the transverse position of vehicles largely affect the aerodynamic force coefficients of vehicles, but the wind velocity basically has no influence on these coefficients. The effects of the number of vehicles and the distance of vehicles from the windward edge on the aerodynamic force coefficients of bridges are strong. When there is a vehicle or no vehicle on the bridge, the aerodynamic force coefficients of the bridge is largely affected, just as do the number of vehicles and the distance of vehicles from the windward edge.

(4) There are still many factors that may affect the aerodynamic force coefficients of the vehicle, such as the configuration of the bridge cross section, the vehicle type, and the running environment (on bridge, embankment, or ground). These factors should be studied to develop empirical formulas to calculate the aerodynamic forces for typical vehicles.

(5) It is known that vehicles on bridges have significant effect on the static aerodynamic forces of the bridge. How much effect of the vehicle on the other aerodynamic forces of the bridge, such as the self-excited force and buffeting force, and on the wind-induced vibrations of the bridge is worth a further study.

It is noted that the aerodynamic force coefficients of the vehicle and the bridge are identified in this paper based on the condition that the vehicle is not moving with respect to the bridge, which does not conform to the actual situation. A new experimental technique considering the vehicle movement should be further investigated and will be reported in a future paper.

Acknowledgements

The authors would like to gratefully acknowledge the supports from the National Science Foundation of China (Project No. 50908025; 51108045; 51178066; 51278069), from the School of Civil Engineering and Architecture, Changsha University of Science and Technology and the Wind Engineering Research Center of Hunan University in China. The third author also appreciates the support from the National Science Foundation of USA (Project CMMI-0927824).

References

Baker, C.J. (1986), “A simplified analysis of various types of wind-induced road vehicle accidents”, *J. Wind Eng. Ind. Aerod.*, **22**(1), 69-85.

Baker, C.J. (1987), “Measures to control vehicle movement at exposed sites during windy periods”, *J. Wind Eng. Ind. Aerod.*, **25**(2), 151-161.

Baker, C.J. (1988), “High sided articulated road vehicles in strong cross winds”, *J. Wind Eng. Ind. Aerod.*, **31**(1), 67-85.

Baker, C.J. (1991a), “Ground vehicles in high cross winds part 1: steady aerodynamic forces”, *J. Fluid. Struct.*, **5**(1), 69-90.

Baker, C.J. (1991b), “Ground vehicles in high cross winds part 2: unsteady aerodynamic forces”, *J. Fluid. Struct.*, **5**(1), 91-111.

Cai, C.S. and Chen, S.R. (2004), “Framework of vehicle-bridge-wind dynamic analysis”, *J. Wind Eng. Ind. Aerod.*, **92**(7-8), 579-607.

Cheli, F., Corradi, R., Diana, G., Tomasini, G. (2004), “A numerical experimental approach to evaluate the aerodynamic effects on rail vehicle dynamics supplement to vehicle system dynamics”, *Dynam. Vehicle.*

Road. Track., **41**, 707-716.

Cheli, F., Desideri, R., Diana, G., Mancini, G., Roberti, R., Tomasini, G. (2006), "Cross wind effects on tilting trains", *Proceedings of the WCRR 2006 7th World Congress on Railway Research*, Montreal, Canada, June 4-8.

Coleman, S.A. and Baker, C.J. (1990), "High side road vehicles in cross winds", *J. Wind Eng. Ind. Aerod.*, **36**(2), 1383-1392.

Coleman, S.A. and Baker, C.J. (1994), "An experimental study of the aerodynamic behaviour of high sided lorries in cross winds", *J. Wind Eng. Ind. Aerod.*, **53**(3), 401-429.

Han, W.S. and Chen, A.R. (2007), "Three-dimensional coupling vibration of wind-vehicle-bridge systems", *China civil engineering journal*, **40**(9), 53-58 (In Chinese).

Han, Y., Cai, C.S., Chen, Z.Q. and Hu, J.X. (2011), "Aerodynamic characteristics of road vehicles and bridges under cross winds", *Proceedings of the 13th International Conference on Wind Engineering*, Amsterdam, the Netherlands.

Li, Y.L., Liao, H.L. and Qiang, S.Z. (2004), "Study on Aerodynamic Characteristics of the Vehicle-bridge System by the Section Model Wind Tunnel Test", *J. China Railway Soc.*, **26**(3), 71-75 (in Chinese) .

Li, Y.L., Qiang, S.Z., Liao, H.L. and Xu, Y.L. (2005), "Dynamics of wind-rail vehicle-bridge systems", *J. Wind Eng. Ind. Aerod.*, **93**, 483-507.

Li, Y.L., Hu, P., Cai, C.S., Zhang, M.J. and Qiang, S.Z. (2012), "Wind tunnel study of a sudden change of train wind loads due to wind shielding effects of bridge towers and passing trains", *J. Eng. Mech. - ASCE* , doi:10.1061/(ASCE)EM.1943-7889.0000559.

Pan, T.C. and Li, J. (2002), "Dynamic vehicle element method for transient response of coupled vehicle-structure systems", *J. Struct. Eng.- ASCE*, **128**(2), 214-223.

Quinn, A.D., Sterling, M., Robertson, A.P. and Baker, C.J. (2007), "An investigation of the wind-induced rolling moment on a commercial vehicle in the atmospheric boundary layer", *Proceedings of the Institution of Mechanical Engineers Part D-Journal of Automobile Engineering*, **221**, 1367-1379.

Scanlan, R. H. and Jones, N.P. (1990), "Aeroelastic analysis of cable-stayed bridges", *J. Struct. Eng.- ASCE*, **116**(2), 279-297.

Suzuki, M., Tanemoto, K. and Maeda, T. (2003), "Aerodynamic characteristics of train/vehicles under cross winds", *J. Wind Eng. Ind. Aerod.*, **91**(1-2), 209-218.

Xu, Y.L. and Guo, W.H. (2003), "Dynamic analysis of coupled road vehicle and cable-stayed bridge system under turbulent wind", *Eng. Struct.*, **25**(4), 473-486.

Yang, Y.B. and Yau, J.D. (1997), "Vehicle-bridge interaction element for dynamic analysis", *J. Struct. Eng. - ASCE*, **123**, 1512-1518.

JH